Position-Sensitive Scanning Fluorescence Correlation Spectroscopy

Joseph P. Skinner, Yan Chen, and Joachim D. Müller
School of Physics and Astronomy, University of Minnesota, Minneapolis, Minnesota 55455

ABSTRACT Fluorescence correlation spectroscopy (FCS) uses a stationary laser beam to illuminate a small sample volume and analyze the temporal behavior of the fluorescence fluctuations within the stationary observation volume. In contrast, scanning FCS (SFCS) collects the fluorescence signal from a moving observation volume by scanning the laser beam. The fluctuations now contain both temporal and spatial information about the sample. To access the spatial information we synchronize scanning and data acquisition. Synchronization allows us to evaluate correlations for every position along the scanned trajectory. We use a circular scan trajectory in this study. Because the scan radius is constant, the phase angle is sufficient to characterize the position of the beam. We introduce position-sensitive SFCS (PSFCS), where correlations are calculated as a function of lag time and phase. We present the theory of PSFCS and derive expressions for diffusion, diffusion in the presence of flow, and for immobilization. To test PSFCS we compare experimental data with theory. We determine the direction and speed of a flowing dye solution and the position of an immobilized particle. To demonstrate the feasibility of the technique for applications in living cells we present data of enhanced green fluorescent protein measured in the nucleus of COS cells.

INTRODUCTION

Along with the introduction of fluorescence correlation spectroscopy (FCS) (1), a similar fluorescence method for the determination of molecular weight of DNA was introduced (2). This method autocorrelates the fluorescence of a rotating sample excited by a stationary laser beam. This and similar FCS techniques that scan multiple volumes are called scanning fluorescence correlation spectroscopy (SFCS). In the past three decades SFCS has taken on a variety of forms and was applied to a number of systems. Briefly, SFCS has been used to correlate spatial fluctuations for particle counting and aggregation measurements (2–6) and also combined with temporal fluctuation analysis to study translational diffusion as well (7,8).

So far, the spatial information embedded in SFCS experiments has not been explicitly considered. To make use of spatial information we synchronize data acquisition and the movement of the scanning excitation beam. By introducing a direct relationship between the fluorescence signal and its position at all times, we are able to introduce position-sensitive SFCS, where correlations are calculated as a function of lag time and position. Although many different scan trajectories are feasible, a scan path that is closed and of simple geometry is needed to allow the derivation of analytically tractable models. A circular scan path is the most straightforward to use. Two parameters characterize its path, the scan radius and the time-dependent phase angle. Because the radius of a circular scan path is constant, each scan position is characterized by its corresponding phase. This allows us to introduce correlation functions that depend on the lag time and the phase. We refer to this technique as position-sensitive SFCS (PSFCS).

This article introduces the theoretical framework of PSFCS and develops models of the correlation function for free diffusion, for diffusion in the presence of uniform flow, and for the case of immobilized particles. We also present experimental data for each case to support our theory. PSFCS and regular SFCS are closely related. The SFCS correlation function is the phase average of the PSFCS correlation function. We first discuss regular SFCS for freely diffusing particles and extend the theory to the case of uniform flow and immobilization. In addition, we show that SFCS is useful for reducing the effects of photobleaching present in FCS correlation data.

By applying the PSFCS technique to a flowing dye solution we are able to determine the diffusion coefficient, the flow direction and the flow speed directly from the experimental data. FCS is unable to detect immobilized particles, because its fluorescence simply adds to the background without introducing fluctuations. PSFCS, on the other hand, is sensitive to immobilized particles, because scanning of the excitation beam across the particle introduces periodic excitation of its fluorescence. We experimentally show that PSFCS allows us to determine the position of an immobilized particle.

A major motivation for developing position-sensitive SFCS lies in the application of the technique inside single cells to characterize diffusion, transport processes, and immobilized proteins. As proof of principle that our technique works in cells we present position-sensitive SFCS data of enhanced green fluorescent protein measured

Submitted February 4, 2005, and accepted for publication May 6, 2005.

Address reprint requests to Joseph P. Skinner, University of Minnesota, School of Physics and Astronomy, 116 Church St., SE Minneapolis, MN 55455. Tel.: 612-624-6045; Fax: 612-624-4578; E-mail: josephs@physics.umn.edu.

0006-3495/05/08/1288/14 $2.00

doi: 10.1529/biophysj.105.060749

in COS cells. The data are described by a model of freely diffusing proteins.

THEORY

To introduce the PSFCS technique we first review the theory behind FCS and SFCS. We begin by describing the relevant expressions to derive the FCS autocorrelation functions for diffusion and flow. SFCS for diffusing particles is then described and also applied to particles in the presence of flow. Finally, we modify the definition of the autocorrelation function and introduce PSFCS. PSFCS is sensitive to the position of the scanned beam. We derive theoretical expressions of the PSFCS correlation functions for diffusion, flow, and immobilization.

FCS

In FCS experiments, fluorescence is collected from very small observation volumes (~1 fL). We express the fluorescence of particles with a particle concentration $C(\vec{r}, t)$ at position $\vec{r}$ and at time t as,

$$F(t) = \kappa \int I^{\mathrm{n}}(\vec{r})\, T(\vec{r})\, C(\vec{r}, t) d\Omega = \kappa \int PSF(\vec{r})\, C(\vec{r}, t) d\Omega, \tag{1}$$

where $I(\vec{r})$ is the intensity of the excitation source at position $\vec{r}$, and $T(\vec{r})$ is the spatial dependence of the collection efficiency of the instrument. The number n equals the number of photons simultaneously absorbed for excitation, $d\Omega$ indicates integration over all space, and the constant κ takes the quantum yield, the extinction coefficient, and the optical detection efficiency into account. In the second equality we introduce the point spread function $PSF(\vec{r})$ of the instrument as the product of the n-th power of the excitation intensity $I(\vec{r})$ and the collection efficiency $T(\vec{r})$ of the instrument.

As particles continuously enter and leave the observation volume, the number of molecules varies and fluctuations in fluorescence is observed. The resulting fluctuations in the fluorescence intensity are defined by (9,10)

$$\delta F(t) = F(t) - \langle F \rangle = \kappa \int PSF(\vec{r}) \delta C(\vec{r}, t) d\Omega, \tag{2}$$

where $\langle F \rangle$ is the time-averaged fluorescence intensity and $\delta C(\vec{r}, t) = C(\vec{r}, t) - \langle C \rangle$ is the concentration fluctuation, with $\langle C \rangle$ being the average concentration of the fluorophores. The fluctuations in the recorded fluorescence signal are used to determine the autocorrelation function,

$$G(\tau) = \frac{\langle \delta F(t) \delta F(t+\tau) \rangle}{\langle F \rangle^2} = \frac{\langle \delta F(0) \delta F(\tau) \rangle}{\langle F \rangle^2}. \tag{3}$$

In the second equality we assumed that the measured physical process is stationary. The correlation function of a stationary process depends only on the time difference τ, which is called the lag time. The autocorrelation function $G(\tau)$ characterizes the average temporal decay of fluorescence fluctuations and provides information about dynamic processes of the fluorophores, such as diffusion times and kinetic reaction coefficients. Theoretical autocorrelation functions are explicitly constructed by inserting Eqs. 1 and 2 into Eq. 3,

$$G(\tau) = \frac{\langle \iint PSF(\vec{r})\, PSF(\vec{r}')\, \delta C(\vec{r}, t)\, \delta C(\vec{r}', t+\tau)\, d\Omega\, d\Omega' \rangle}{\left[\langle C \rangle \int PSF(\vec{r}) d\Omega \right]^2}, \tag{4}$$

where $\vec{r}$ and $\vec{r}'$ correspond to positions at time t and $t+\tau$, respectively. We model the PSF of the instrument as the n-th power of a three-dimensional Gaussian (3DG) function,

$$PSF_{\mathrm{3DG}}(x, y, z) = A^{\mathrm{n}} \exp\left[-\frac{2n(x^2+y^2)}{w_0^2} - \frac{2nz^2}{z_0^2} \right]. \tag{5}$$

Here A is the maximum intensity of the beam, w_0 is its beam waist, and z_0 describes the axial length of the excitation volume. We introduce the parameter a as the ratio of the axial/radial beam waist $a = z_0/w_0$. The autocorrelation function for the case of freely diffusing fluorophores and a 3DG PSF is then,

$$G_{\mathrm{D}}(\tau) = G(0) \frac{1}{(1+\tau/\tau_{\mathrm{D}}) \sqrt{1+\tau/a^2\tau_{\mathrm{D}}}}, \tag{6}$$

where the diffusion time is given by $\tau_{\mathrm{D}} = w_0^2/4nD$ and D is the diffusion coefficient of the fluorophore. The fluctuation amplitude $G(0)$ is inversely proportional to the average number of molecules N in the observation volume, $G(0) = \gamma/N$, where the shape factor γ depends on the shape of the PSF. The shape factor for a three-dimensional Gaussian function is $1/(2\sqrt{2})$.

For systems of particles undergoing diffusion and uniform flow with velocity $\vec{v}$, the concentration is governed by

$$\frac{\partial C(\vec{r}, t)}{\partial t} = -D\nabla^2 C(\vec{r}, t) - \vec{v}_{\mathrm{F}} \nabla C(\vec{r}, t). \tag{7}$$

Without loss of generality we will assume that the flow is in the positive y-direction, $\vec{v}_{\mathrm{F}} = v_{\mathrm{F}}\hat{y}$. This equation can be used to calculate the functional form of the autocorrelation function $G_{\mathrm{DF}}(\tau)$ for diffusion and flow as has been outlined previously (10,11),

$$G_{\mathrm{DF}}(\tau) = G_{\mathrm{D}}(\tau) \exp\left[-\frac{(\tau/\tau_{\mathrm{F}})^2}{1+\tau/\tau_{\mathrm{D}}} \right] = G_{\mathrm{D}}(\tau) F(\tau). \tag{8}$$

The autocorrelation function $G_{\mathrm{DF}}(\tau)$ is the product of the function $G_{\mathrm{D}}(\tau)$ and the flow factor $F(\tau)$. We also introduced

the flow time $\tau_F = w_0/\sqrt{n}\,v_F$, which characterizes the time it takes for crossing the PSF by flow alone.

It is often sufficient to describe experimental data using a two-dimensional Gaussian function. We arrive formally at this function by taking the limit of the 3DG function where the beam waist ratio goes to infinity, $a \to \infty$. The autocorrelation function for the two-dimensional Gaussian PSF model is similarly derived from Eqs. 6 and 8 by taking the limit, $a \to \infty$.

SFCS

So far we have discussed the case of a stationary PSF. In SFCS the PSF is no longer stationary and depends on time. We describe SFCS for the simple case of a circular scan pattern, with the scan vector,

$$\vec{r}_s(t) = r_s \cos(\phi_0 + \omega t)\hat{x} + r_s \sin(\phi_0 + \omega t)\hat{y}, \qquad (9)$$

which rotates the center of the PSF through a circular orbit with angular frequency ω and scan radius r_s. The phase ϕ_0 determines the position of the PSF at the start of the scan when $t = 0$. Any stationary point spread function $PSF(\vec{r})$ can be transformed into a scanning-FCS point spread function by $PSF(\vec{r} - \vec{r}_s(t))$. The three-dimensional Gaussian PSF, for example, has the following functional form in the case of circular scanning,

$$PSF(x,y,z,t) = A^n \exp\left[-\frac{2n\left((x - r_s\cos(\phi_0+\omega t))^2 + (y - r_s\sin(\phi_0+\omega t))^2\right)}{w_0^2} - \frac{2nz^2}{z_0^2}\right]. \qquad (10)$$

SFCS for diffusion

For particles undergoing random translational diffusion with a diffusion coefficient D, the functional form of the SFCS autocorrelation function can be calculated by inserting Eq. 10 into Eq. 4. The following expression results (4):

$$G_s(\tau) = G_D(\tau)S_D(\tau). \qquad (11)$$

The autocorrelation function for SFCS can be factored into two functions; the regular correlation function for diffusing particles $G_D(\tau)$ in the absence of scanning (Eq. 6) and a scan factor for diffusing particles (4),

$$S_D(\tau) = \exp\left[-\frac{4n\rho^2\,\mathrm{Sin}(\omega\tau/2)^2}{1+\tau/\tau_D}\right]. \qquad (12)$$

Equation 12 introduces the dimensionless scaled radius $\rho = r_s/w_0$. The scan factor modulates the autocorrelation function as shown in Fig. 1 *A*. The unscanned correlation function $G_D(\tau)$ (*dashed line*) is the envelope of the scanned correlation function $G_s(\tau)$ (*solid line*) (Fig. 1 *A*). One can see that as the scan radius goes to zero, $\rho \to 0$, the scan factor approaches unity, $S_D(\tau) \to 1$, thereby reducing the autocorrelation function in Eq. 11 to the special case of the unscanned correlation function.

SFCS for uniform flow and diffusion

We derived the autocorrelation function $G_{SDF}(\tau)$ for SFCS in the presence of uniform flow in addition to diffusion,

$$G_{SDF}(\tau) = G_{DF}(\tau)S_D(\tau)I_0\left[\frac{4\sqrt{n}\rho\tau\sin(\omega\tau/2)}{\tau_F(1+\tau/\tau_D)}\right] = G_{DF}(\tau)S_{DF}(\tau), \qquad (13)$$

where the function $I_0[x]$ refers to the zeroth-order modified Bessel function of the first kind with argument x. We see that $G_{SDF}(\tau)$ is the product of the autocorrelation function in the absence of scanning (Eq. 8) and the scan factor $S_{DF}(\tau)$ for the diffusion and flow model. This scan factor is defined as the product of the Bessel function and the scan factor for diffusion (Eq. 12). In the limiting case where flow is very slow or nonexistent, $\tau_F \to \infty$, both the Bessel function and

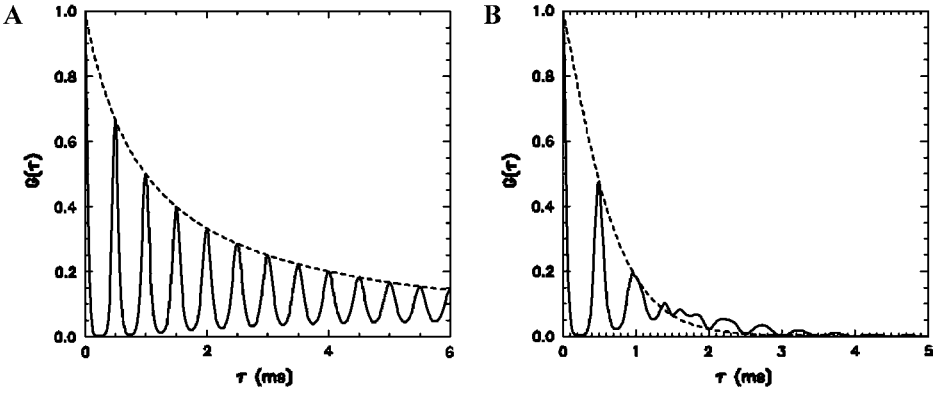

FIGURE 1 Theoretical curves for SFCS for diffusion and diffusion with flow. (*A*) For the diffusion-only case the FCS autocorrelation function (*dashed line*) is the envelope of the SFCS curve (*solid line*). Correlation functions are modeled for $\tau_D =$ 1 ms, $\rho = 1$, and $\omega = 2\pi f$, where $f = 2$ kHz. (*B*) In the presence of flow the SFCS function (*solid line*) is not enveloped by the FCS correlation function (*dashed line*). The correlation was calculated for a flow time of $\tau_F = 1$ ms, whereas the other parameters are the same as for panel A.

the flow factor approach unity and Eq. 13 reduces to Eq. 11, the SFCS autocorrelation function for diffusing particles. A plot of the autocorrelation function described by Eq. 13 is shown in Fig. 1 *B* along with the unscanned autocorrelation function for flow and diffusion (*dashed line*). The flow time in this model is set to 1 ms. Note that, contrary to the diffusion-only case, the SFCS autocorrelation function $G_{\mathrm{SDF}}(\tau)$ is not enveloped by the unscanned correlation function $G_{\mathrm{DF}}(\tau)$ for all correlation times. The unscanned correlation function crosses the SFCS autocorrelation function at $\tau \sim 1.4$ ms and starts to envelope its minima. This increase in the correlation amplitude is a result of particles flowing across the scan circumference. The particles that appear at the opposite side of the scan circumference, 180° from the initial point of entry, are intercepted by the scanned beam providing an additional source for correlations not present in the unscanned case. The transition time is determined by the time a particle needs to travel across the diameter of the scan trajectory. At earlier times the majority of particles are still confined within the volume of the PSF. These particles are revisited by the laser beam every scan period, which gives rise to the peaks in the correlation amplitude.

Position-sensitive SFCS

Scanning of the excitation beam leads to a time-dependent location of the PSF. The center of the PSF is described by the time-dependent scan vector $\vec{r}_{\mathrm{s}}(t)$. Assuming a circular scan path, the scan vector $\vec{r}_{\mathrm{s}}(t)$ is conveniently expressed by its length r_{s} and a time-dependent phase angle,

$$\phi_{\mathrm{PSF}}(t) = (\phi_0 + \omega t) \mod 2\pi. \tag{14}$$

The angle varies continuously with time between 0 and 2π and the phase offset ϕ_0 characterizes the position of the PSF at $t = 0$ (Fig. 2). This offset is experimentally controlled by synchronization of the scanning electronics and the data acquisition card. We may formally write the fluorescence

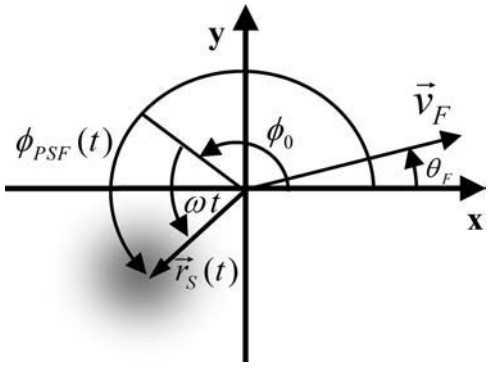

FIGURE 2 Depiction of the position-sensitive coordinate system. The coordinate system shows how the different angles relevant to the PSF position and the flow vector are defined in a right-handed coordinate system.

$F(\phi_{\mathrm{PSF}}, t)$ and its fluctuation $\delta F(\phi_{\mathrm{PSF}}, t)$ as dependent on both time t and phase angle ϕ_{PSF}. As time increases the PSF scans its circular trajectory returning to its initial position with a period of $2\pi/\omega$. Thus, we may describe physical properties associated with a particular spatial position of the PSF by autocorrelating the fluorescence fluctuations with respect to a particular phase angle ϕ. Consider an arbitrary function $f(\phi_{\mathrm{PSF}}(t), t)$, which depends both on time and the angle. We define the average of $f(\phi_{\mathrm{PSF}}(t), t)$ with respect to a particular phase ϕ by,

$$\langle f \rangle_\phi = \frac{\int_{t=0}^{T} f(\phi_{\mathrm{PSF}}(t), t)\, \delta(\phi_{\mathrm{PSF}}(t) - \phi) dt}{\int_{t=0}^{T} \delta(\phi_{\mathrm{PSF}}(t) - \phi) dt}. \tag{15}$$

The function $f(\phi_{\mathrm{PSF}}(t), t)$ is integrated over the complete measurement time T. The δ-function $\delta(\phi_{\mathrm{PSF}}(t) - \phi)$ ensures that only times with the proper phase are picked during the integration process.

The standard definition of the autocorrelation function (Eq. 3) used by SFCS ignores the phase information. However, we would like to use this information and therefore define two types of fluctuations that will depend upon the phase,

$$\delta F(\phi, t) = F(\phi, t) - \langle F \rangle, \tag{16}$$

$$\delta \tilde{F}(\phi, t) = F(\phi, t) - \langle F \rangle_\phi. \tag{17}$$

The fluctuation $\delta F(\phi, t)$ measures the deviation from the averaged fluorescence $\langle F \rangle$, whereas $\delta \tilde{F}(\phi, t)$ characterizes the deviation of the signal from the average fluorescence $\langle F \rangle_\phi$ at the phase angle ϕ. This allows us to define two different position-sensitive correlation functions,

$$G_\phi(\phi, \tau) = \frac{\langle \delta F(\phi_{\mathrm{PSF}}(t), t) \delta F(\phi_{\mathrm{PSF}}(t+\tau), t+\tau) \rangle_\phi}{\langle F \rangle^2}, \tag{18}$$

$$\tilde{G}_\phi(\phi, \tau) = \frac{\langle \delta \tilde{F}(\phi_{\mathrm{PSF}}(t), t) \delta \tilde{F}(\phi_{\mathrm{PSF}}(t+\tau), t+\tau) \rangle_\phi}{\langle F \rangle_\phi \langle F \rangle_{\phi+\omega\tau}}. \tag{19}$$

Equations 18 and 19 require a stationary fluorescence signal, so that the correlation function only depends on time differences τ. Both position-sensitive functions characterize the correlation between fluorescence fluctuations at phase position ϕ with the fluctuations occurring a time τ later at phase position $\phi + \omega\tau$, but differ in the denominator. The function $G_\phi(\phi, \tau)$ normalizes the correlation of the fluctuations to the square of the total average fluorescence $\langle F \rangle$, whereas $\tilde{G}_\phi(\phi, \tau)$ normalizes the fluctuations to $\langle F \rangle_\phi$ and $\langle F \rangle_{\phi+\omega\tau}$, which describes the average fluorescence at phase positions ϕ and $\phi + \omega\tau$. We refer to Eq. 19 as the phase-normalized correlation function. The differences between both correlation functions will be discussed in more detail later when we consider the correlation of deterministic signals. For the moment we would like to point out that

averaging the position-sensitive autocorrelation function $G_\phi(\phi,\tau)$ over all phase angles returns the standard SFCS autocorrelation function,

$$G_S(\tau) = \frac{1}{2\pi}\int_0^{2\pi} G_\phi(\phi,\tau)\,d\phi = \frac{\langle \delta F(0)\delta F(\tau)\rangle}{\langle F\rangle^2}. \qquad (20)$$

Averaging the phase-angle normalized correlation function $\tilde{G}_\phi(\phi,\tau)$ over all phase angles only returns the standard SFCS autocorrelation function, if the average fluorescence is independent of angle, $\langle F\rangle = \langle F\rangle_\phi$.

PSFCS for uniform flow and diffusion

We define the flow velocity vector $\vec{v}_F = v\cos\theta_F\,\hat{x} + v\sin\theta_F\,\hat{y}$, where the flow angle θ_F is measured counterclockwise as shown in Fig. 2. The position-sensitive autocorrelation function, calculated from Eq. 19 is,

$$\tilde{G}_\phi(\phi,\tau) = G_{DF}(\tau)S_D(\tau) \exp\left[\frac{4\sqrt{n}\rho\tau\sin(\omega\tau/2)\sin(\theta_F-\omega\tau/2-\phi)}{\tau_F(1+\tau/\tau_D)}\right]. \qquad (21)$$

Equation 21 describes the correlation between the phase angle ϕ and the phase angle $\phi+\omega\tau$ as a function of lag time τ. During the lag time τ particles diffuse and flow in the direction of $\vec{v}_F$, while the position of the PSF advances in phase by $\omega\tau$.

In the presence of flow, the structure of the PSFCS curve depends on the chosen phase angle. To illustrate this dependence Fig. 3, *A* and *B*, show position-sensitive autocorrelation curves in the presence of flow along the x axis ($\theta_F = 0$) for a phase of $\phi = \pi$ and $\phi = 0$, respectively. The correlation is graphed as a function of lag time τ along the bottom axis. The corresponding change in phase angle $\omega\tau$ is displayed on the top axis. The correlation function was calculated for a flow time of $\tau_F = 1$ ms, a scaled radius of $\rho = 1$, a diffusion time of $\tau_D = 1$ ms, and a scan frequency of 2 kHz. The dashed line represents the regular, unscanned correlation function in the presence of flow and diffusion using the same parameters as for the position-sensitive correlation functions. Per definition, both FCS and PSFCS functions must be equal for phase angles that are integer multiples of 2π. However, the regular correlation function envelops the scanned correlation function for a phase of $\phi = 0$ (Fig. 3 *B*), but this is not the case for a phase of $\phi = \pi$. As shown in Fig. 3 *A* the regular correlation function envelops the maxima of $G_\phi(\pi,\tau)$ at early correlation times, whereas at later times it envelops the minima of $G_\phi(\pi,\tau)$. This behavior is similar to the situation encountered in SFCS and is a consequence of the presence of flow.

To understand the structural changes of the PSFCS autocorrelation function with phase angle from a physical point of view, we first consider the case $\phi = \pi$ (see Fig. 3 *A*). Correlations are determined with respect to position A (see *inset* of Fig. 3 *A*). Flow is moving particles in the positive x-direction. It takes a time of $\rho\tau_F$ for particles to cross the entire scan circumference by flow, i.e., from point A to point B in the figure. At early times ($\tau \ll \rho\tau_F$) particles are still within the vicinity of point A. Every time the PSF returns to point A, it revisits the particles, which results in maxima of the correlation amplitude. The average particle will move along the x axis toward the opposite side of the scan circumference, π radians away from point A. The particles are intercepted by the moving PSF as they cross point B. Revisiting of the particles at point B instead of at point A results in a shift of the maxima of the correlation amplitude by π for $\tau > \rho\tau_F$. Because A is the point on the scan circumference that is furthest away from the average position of the particles for $\tau > \rho\tau_F$, the correlation function exhibits a minimum whenever point A is revisited. Because FCS and position-sensitive SFCS correlation functions are identical for phase angles that are integer multiples of 2π, the minima are now enveloped by the FCS curve.

Now, let us consider correlations calculated with respect to $\phi = 0$ (see Fig. 3 *B*). Flow directs the particles away from the entire scan circumference (see *inset* of Fig. 3 *B*). In other words, the average particle trajectory will not cross the scan path at later times. Because position B will always be the closest to the average location of the particle, maxima of the correlation amplitude occur for phase angles that are integer multiples of 2π. Note that the amplitude of the correlation function decays faster for a phase angle of $\phi = 0$ than for $\phi = \pi$. This is because particles move, on average, away from the entire scan circumference for $\phi = 0$, whereas they first move across the scan circle before moving away for $\phi = \pi$.

These structural changes in the position-sensitive correlation signal as a function of phase angle invite one to perform a global analysis of data, where all possible phase angles are considered. This approach leads to two-dimensional correlation functions. Fig. 3 *C* shows the surface plot of Eq. 21 as a function of lag time τ and phase angle ϕ. Its contour is plotted in Fig. 3 *D*. These plots show the structural change that occurs by calculation of correlations as a function of space and time in the presence of flow. By looking at the contour, we see that the greatest structural change and overall slowest decay occurs at $\phi = \pi$ corresponding to particles flowing across the center of the scanning circle. At the other extreme, $\phi = 0$, decay is clearly much faster.

PSFCS for diffusion

We now examine the case of a diffusing species in the absence of flow. The position-sensitive SFCS correlation function is formally derived from Eq. 21 by taking the limit $\tau_F \to \infty$,

$$G_\phi(\phi,\tau) = G_D(\tau)S_D(\tau). \qquad (22)$$

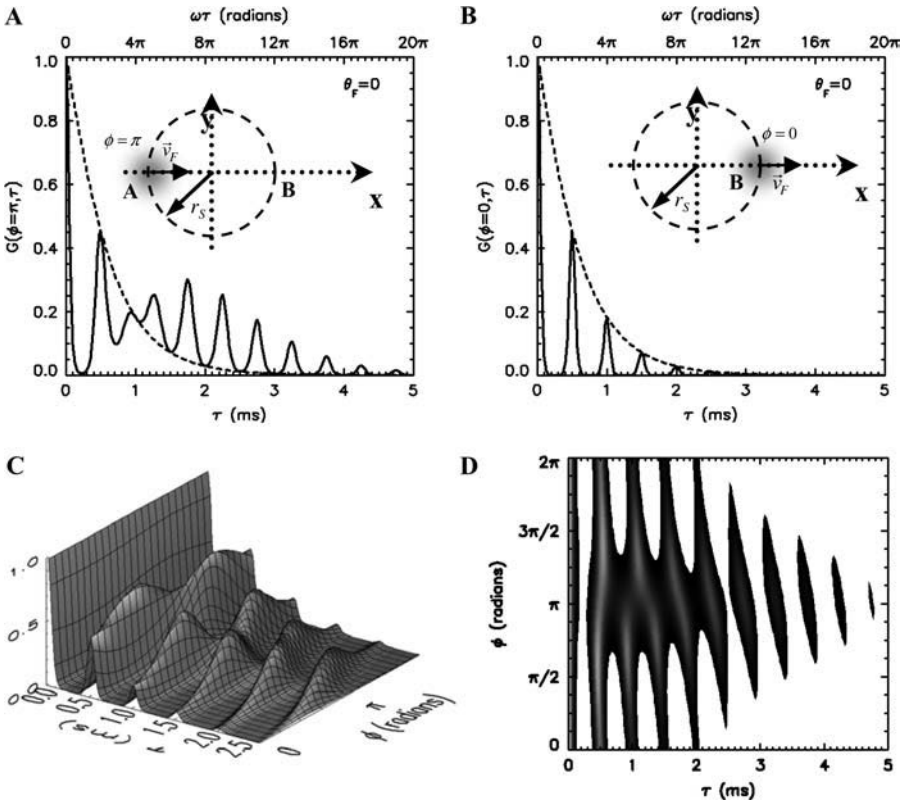

FIGURE 3 $G(\phi,\tau)$ for flow with $\theta_F = 0$. (*A*) For $\phi = \pi$ the PSFCS correlation function (*solid line*) exceeds the FCS autocorrelation (*dashed line*) when particles had enough time to move from point A to point B (see *inset*). (*B*) For $\phi = 0$ the PSFCS autocorrelation curve is enveloped by the FCS autocorrelation curve. Flow transports particles away from point B without ever crossing the scan circumference. The correlation surface as a function of lag time and phase angle is shown (*C*) along with its contour (*D*). The flow direction is identified by the fastest decay of the correlation as a function of phase angle. The parameters used for the model are the same as for Fig. 1.

The correlation function for a purely diffusing species is independent of the phase angle ϕ, as expected, because the diffusion process is isotropic. As a consequence of this independence from the phase angle the PSFCS correlation function is identical to the regular SFCS correlation function shown in Eq. 11.

$$I(\vec{r},t) = PSF(\vec{r} - \vec{r}_s(\phi,t))\lambda\delta\left(\vec{r} - \vec{r}_p\right), \tag{24}$$

where λ represents the photon count rate of the particle when located at the center of the PSF. Inserting Eq. 24 into Eq. 18 results in the following form of the autocorrelation function:

$$G_{\text{imm}}(\phi,\tau) = \frac{(\exp[-2n\alpha\rho\cos(\gamma)] - \mathrm{I}_0[2n\alpha\rho])(\exp[-2n\alpha\rho\cos(\gamma - \omega\tau)] - \mathrm{I}_0[2n\alpha\rho])}{(\mathrm{I}_0[2n\alpha\rho])^2}, \tag{25}$$

PSFCS for an immobilized particle

In contrast to the correlation function for a stationary PSF, the scanned autocorrelation function is sensitive to immobilized particles. An orbiting PSF sweeps across the immobilized particle and excites it. This creates an intensity trace characterized by a peak repeating every scan period due to the fluorescence of the localized particle. To use the position-sensitive technique on an immobilized particle, we use the fluctuations defined by Eq. 16 and calculate the position-sensitive autocorrelation function according to Eq. 18 for a single particle located at

$$\vec{r}_p = a\cos\theta\hat{x} + a\sin\theta\hat{y}, \tag{23}$$

in the *XY* plane. The parameters a and θ are the radial and angular positions of the particle, respectively. The fluorescence intensity of the immobilized particle is described by

where $\alpha = a/w_0$ and $\gamma = \theta - \phi$. Knowledge of the scan radius allows the determination of the particle's position from its polar coordinates a and θ by fitting of experimental data. Note that the standard autocorrelation function for the immobilized particle is determined by averaging Eq. 25 about the angle ϕ (see Eq. 20),

$$G_{\text{imm}}(\tau) = \frac{I_0[4n\alpha\rho\cos(\omega\tau/2)]}{(I_0[2n\alpha\rho])^2} - 1. \tag{26}$$

We would like to point out that fluctuations as defined by Eq. 17 are not suitable for correlating the signal from an immobilized particle. The fluorescence signal of an immobilized particle is deterministic, in contrast to the random signal of a diffusing particle. The fluorescence only depends on the phase angle and is independent of time. In other words, the instantaneous and average fluorescence at phase

angle ϕ are equal, $F(\phi,t) = \langle F \rangle_\phi$, and their fluctuations vanish, $\delta\tilde{F}(\phi,t) = 0$. The disappearance of fluctuations leads to a vanishing phase-normalized correlation function $\tilde{G}_\phi(\phi,\tau)$. However, this property is useful to separate fluctuations due to immobilized sources and fluctuations arising from stochastic processes within the same system. This will be discussed in more detail later.

PSFCS for independent species

In many experiments a mixture of species is present. If the species are statistically independent from one another, then the autocorrelation function is a superposition of the autocorrelation functions of each species. In regular FCS, the autocorrelation function of each species is weighed by the square of its fractional intensity (Thompson, 1991). It is straightforward to show that the position-sensitive autocorrelation $G_\phi(\phi,\tau)$ of a mixture follows the same relationship

$$G_\phi(\phi,\tau) = \sum_i \frac{\langle F_i \rangle^2}{\langle F_{tot} \rangle^2} G_{i,\phi}(\phi,\tau) = \sum_i f_i^2 G_{i,\phi}(\phi,\tau), \quad (27)$$

where f_i is the fractional intensity of the i-th species. The phase-normalized correlation function $\tilde{G}_\phi(\phi,\tau)$ of a mixture is also given by a superposition of the correlation functions of each species $G_{i,\phi}(\phi,\tau)$,

$$\begin{aligned}\tilde{G}_\phi(\phi,\tau) &= \sum_i \frac{\langle F_i \rangle_\phi \langle F_i \rangle_{\phi+\omega\tau}}{\langle F_{tot} \rangle_\phi \langle F_{tot} \rangle_{\phi+\omega\tau}} \tilde{G}_{i,\phi}(\phi,\tau) \\ &= \sum_i f_{i,\phi} f_{i,\phi+\omega\tau} \tilde{G}_{i,\phi}(\phi,\tau), \end{aligned} \quad (28)$$

but the weighing factor of the i-th species is given by the product of the fractional intensity $f_{i,\phi}$ at phase ϕ and the fractional intensity $f_{i,\phi+\omega\tau}$ at phase $\phi+\omega\tau$.

MATERIALS AND METHODS

Experimental setup and procedures

Experiments were conducted on a homebuilt two-photon fluorescence fluctuation microscope. The two-photon excitation source is a mode locked titanium-sapphire laser (Tsunami, Spectra Physics, Mountain View, CA) pumped with an intracavity doubled Nd:YVO_4 (Spectra Physics) laser. The laser beam is scanned in a circle using an X-Y galvonometer scanner (model 6350, Cambridge Technology, Cambridge, MA) driven by a computer-controlled arbitrary waveform generator (AWG) (PC instruments, Lawrence, KA). The beam passes through a beam expander before entering a modified Axiovert 200 microscope (Zeiss, Göttingen, Germany). A 63× oil immersion objective with a numerical aperture of 1.4 (Zeiss) focuses the laser light into the sample. Fluorescence is collected with the same objective. A dichroic filter (675DCSXR, Chroma Technology, Brattleboro, VT) separates the fluorescence from the excitation light. The fluorescence after passing through a tube lens is descanned with a 10× microscope objective (CP-Achromat N.A. = 0.24, Zeiss) for SFCS experiments. A PMT (model H7421-40, Hamamatsu City, Japan) positioned at the afocal plane detects the light. For instrument calibration experiments an APD (model SPCM-AQR-14, Perkin Elmer, Vaudreuil, Canada) was positioned at the focal point of the tube lens to measure fluorescence. The TTL pulses produced by the PMT or APD were registered in an FCS data acquisition card (ISS, Champaign, IL) and stored in computer files for analysis. For the position-sensitive measurements the FCS card and AWG board are synchronized by clocking them with two phase-locked function generators (HP3325A and 33250A, Hewlett Packard/Agilent Technologies, Palo Alto, CA) operating at frequencies that are integer multiples of one another to ensure that each scan cycle corresponds to an integer number of measured data points.

All experiments were conducted with an excitation wavelength of 780 nm and a power at the sample of ~2 mW or less. Data were collected for ~2 min for all experiments presented. The scan frequency used for the experiments was 2 kHz. The scan radius was calibrated by focusing the light through a 10× objective onto a position-sensitive device (PSD) (Pacific Silicon Sensors, Westlake Village, CA) mounted on the microscope. The corresponding scan radius for the 63× objective was obtained by dividing the measured value for the 10× objective by 6.3. To accurately determine the position of the scanned beam at all times, we monitored the phase delay between the electronic input signal of the driver of the galvanic mirrors and the output of the PSD device with an oscilloscope at 2 kHz. The observed phase delay was taken into account in the analysis of the data. The beam waist was calibrated from measurements of fluorescein in an eight-well slide (Nalge Nunc International, Naperville, IL) with an APD. The experimental autocorrelation curve was fit to theory using a fixed diffusion coefficient of 300 $\mu m^2/s$ to determine the beam waist of the instrument. Measurement of EGFP was conducted in an eight-well slide as well. For flow experiments, Teflon tubing was connected to both sides of a square borosilicate capillary (800 μm inner diameter) (Vitrocom, Mountain Lakes, NJ), which was mounted on the microscope. Sample solution was loaded into a syringe and connected to one end of the tubing. By varying the height of the input syringe and the output tube a pressure gradient is produced that initiates flow.

Sample preparations

Fluorescein and Alexa488 (Molecular Probes, Eugene, OR) dyes were diluted to nanomolar concentration. The stock concentrations of dyes were determined by absorption spectroscopy using the extinction coefficient quoted by the manufacturer. Fluorescein was diluted in a phosphate buffer (pH = 8.5). Alexa488 dye was diluted in a solution containing ~60% glycerol (Roche, Indianapolis, IN) and ~40% water. For in vitro measurements, EGFP protein was purified according to Patterson et al. (12) and diluted in phosphate buffer (Dulbecco's phosphate buffered saline, Cambrex, Walkersville, MA). To measure EGFP in vivo, COS-1 cells were transiently transfected, and fluorescence of EGFP was recorded in the cell nucleus. Samples for immobilization experiments were prepared by drying 26-nm fluorescent spheres (Duke Scientific, Palo Alto, CA) on the coverslip of an eight-well slide. Alexa488 solution was later added to the well introducing a second, randomly diffusing species.

Data analysis

To analyze data using the position-sensitive technique, we developed a new algorithm for calculating the autocorrelation, which was implemented in a program written for IDL (Research Systems, Boulder, CO). The new program was tested using unscanned data from a fluorescent dye solution. The algorithm gave the same results as the standard autocorrelation algorithm.

Fitting was done using the Levenberg-Marqaurt method in Mathematica (Version 4.2, Wolfram Research, Champaign, IL). To weight the fits, a data set was divided into 10 segments from which 10 autocorrelation curves were calculated. The standard deviation for each data point was calculated across the 10 autocorrelation functions and used to assign errors to points in curves generated from the entire data set. The errors quoted for the fit parameters are the square roots of the diagonal terms of the error matrix (13) unless otherwise noted. Calibration measurements yielded a value of $a = 5.5$ using a three-dimensional Gaussian PSF. Comparison to the two-dimensional Gaussian resulted in deviations ~5% for τ_D and <1% for τ_F and ρ. These values are within the experimental error and therefore fitting was done using the two-dimensional Gaussian PSF.

RESULTS

SFCS

SFCS data were obtained for Alexa488 in the glycerol/water solution. A sinusoidal signal with amplitude of 150 mV and frequency of 2 kHz was applied to the galvanic scan mirrors. We collected regular FCS data without scanning as control. The triangles in Fig. 4 represent the regular autocorrelation function. A fit to Eq. 6, assuming a two-dimensional Gaussian PSF returned a diffusion time of 0.45 ms. The SFCS data (*diamonds*) were fit to Eq. 11 assuming a two-dimensional Gaussian PSF with the diffusion time fixed to 0.45 ms, in accordance with the previous measurement. Fig. 4 shows the fitted SFCS curve (*solid line*) together with its residuals. The regular correlation function envelopes the scanned autocorrelation function as expected. The fit gives $\rho = 1.09 \pm 0.01$. Using the beam waist from calibration of 0.37 ± 0.03 μm this yields a radius of 0.40 ± 0.03 μm. This is in good agreement with the independent measurement using the PSD mounted on the microscope, which led to a radius of 0.37 ± 0.05 μm.

SFCS and photobleaching

The ability to recognize and control photobleaching in FCS experiments is important. Photobleaching in one-photon excitation is easily spotted by the telltale reduction in the average fluorescence signal during the measurement because of the depletion in fluorophores along the path of the laser beam. Photobleaching during two-photon excitation is strictly limited to the vicinity of the focal volume. Consequently, no reduction in fluorescence intensity is observed during the experiment even in the presence of severe photobleaching. However, the decay of the autocorrelation function speeds up because of bleaching, which leads to unphysical parameters if not recognized. For example, the fitted diffusion time decreases as photobleaching leads to a more quickly decaying correlation function.

Scanning of the PSF through the sample may be used to reduce the effects of photobleaching. To show this, a power study was performed using FCS and SFCS measurements on EGFP in aqueous solution at the approximate powers of 0.5, 1.5, and 1.75 mW. Selected experimental correlation curves from this study are shown in Fig. 5. The diamonds represent the correlation function obtained for a power of 1.75 mW at the sample, and the solid line through the data is a fit to a regular diffusion model. In addition, we show the fit to the correlation function from the FCS data taken at 0.5 mW as the dashed line. This correlation function decays more slowly than the curve taken at the higher power of 1.75 mW, thereby indicating the presence of photobleaching in the data taken at 1.75 mW.

The SFCS correlation function measured at a power of 1.75 mW, while scanning the beam, is shown as the squares in Fig. 5. Clearly, the scanning autocorrelation function is

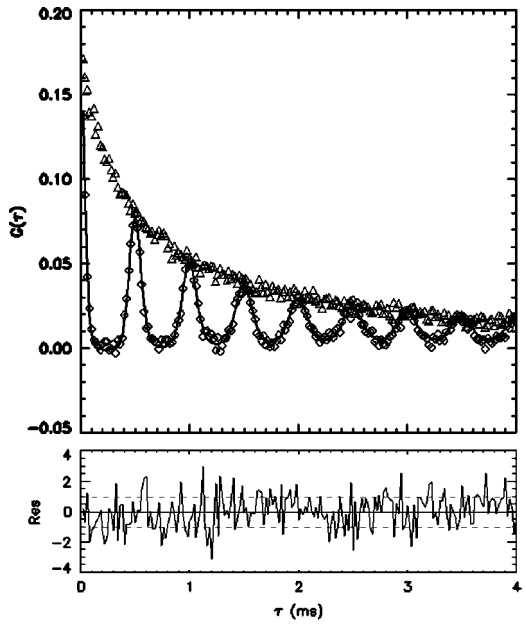

FIGURE 4 SFCS data of a diffusing dye solution. Alexa488 in glycerol solution was scanned at a frequency of 2 kHz and an amplitude of 150 mV. The FCS autocorrelation curve (△) is the envelope of the SFCS autocorrelation curve (◇). The fit (*solid line*) gives $\rho = 1.09 \pm 0.01$ for the scaled radius and a reduced χ^2 of 1.3. The normalized residuals for fitting the SFCS curve are shown below.

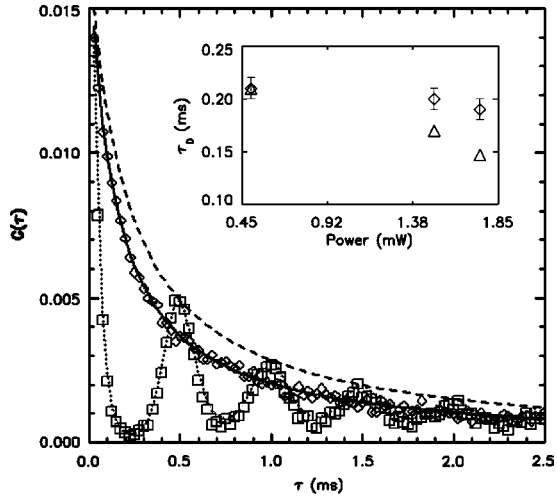

FIGURE 5 SFCS and FCS correlation functions of EGFP at different powers. The dashed line shows the fit to an FCS curve taken with a power of ~0.5 mW at the sample with a diffusion time of $\tau_D = 0.21 \pm 0.01$ ms. Another FCS measurement of the same sample was taken at a higher power (~1.75 mW). A fit (*solid line*) of the correlation function (◇) to a diffusion model returned an apparent diffusion time of $\tau_D = 0.15 \pm 0.01$ ms. The dotted line represents a fit of SFCS data (□) taken at the same power (~1.75 mW) and determined a diffusion time of $\tau_D = 0.19 \pm 0.01$ ms. The fitted diffusion time as a function of power is shown as an inset. The diffusion time of the FCS measurements (△) decreases by 30% over the power range studied because of the onset of photobleaching. The diffusion time of SFCS experiments (◇) on the other hand is significantly more robust.

not enveloped by the regular correlation function taken at the same power (*diamonds*), as the theory suggests, but is enveloped by the regular correlation function measured at the lower power of 0.5 mW (*dashed line*). The fitted diffusion times of the FCS and SFCS data provide a characterization of the severity of photobleaching and are shown in Fig. 5 (*inset*) as a function of power. Each power study was conducted twice and the averaged diffusion time is plotted (reduced $\chi^2 \sim 1.5$ for the fits). The diffusion time measured for FCS experiments (*triangles*) decreases as a function of power from a value of 0.21 ± 0.01 ms at 0.5 mW to a value of 0.15 ± 0.01 ms at a power of 1.75 mW. This decrease in the diffusion time by ~30% indicates the onset of photobleaching. The diffusion time measured for SFCS experiments (*diamonds*) decreases from a value of $0.21 \pm 0.01 - 0.19 \pm 0.01$ ms over the power range studied, which corresponds to a reduction of only ~10%, which is within experimental error. These data clearly demonstrate that SFCS is less sensitive to photobleaching than regular FCS experiments. By scanning the PSF through the sample, the proteins are less likely to bleach during the shortened time in which they are in the excitation volume.

Scanning and flow

An Alexa488 glycerol/water solution was used to perform flow experiments in a capillary. The following sequence of experiments was performed for each sample. First, position-sensitive SFCS data were taken in the presence of flow. Then, scanning was stopped, and regular FCS data were obtained for the flowing sample. Next, flow was stopped by closing a valve situated between the syringe and the capillary. We acquired regular FCS data to provide an independent measure of the diffusion time. Finally, with flow still stopped, SFCS data were taken.

Correlation functions from regular FCS measurements with flow (*diamonds*) and without flow (*triangles*) are shown in Fig. 6 *A*. We fit the correlation curve taken in the absence of flow and obtain a diffusion time of 0.72 ± 0.02 ms. Next, we fit the correlation function determined in the presence of flow to Eq. 8 with the diffusion time fixed to 0.72 ms and obtain a flow time of 0.64 ± 0.01 ms. The SFCS correlation function from the data taken with flow (*diamonds*) is presented in Fig. 6 *B* together with a fit (*solid line*) to Eq. 13 with $\rho = 0.97$. The fit determined a diffusion time of $\tau_D = 0.65 \pm 0.06$ ms and a flow time of $\tau_F = 0.61 \pm 0.01$ ms, which are in good agreement with the parameters determined from regular FCS experiments. Fig. 6 *B* also shows the fit to the corresponding regular FCS correlation function as a dotted line. The correlation function in the absence of scanning envelopes the maxima, then crosses the SFCS correlation function and finally envelopes its minima, as predicted by theory.

Determination of direction using PSFCS

We again measured a sample of Alexa488 in the presence and absence of flow while scanning the beam. First, the position-sensitive correlation function of the data taken in the absence of flow was determined and is shown in Fig. 7 *A*. The shaded region shows the experimental autocorrelation function as a function of both phase angle ϕ and the lag time τ. The experimental correlation function is only plotted for phase angles between 0 and π to more clearly show the fit that is represented by the mesh covering all phase angles from 0 to 2π. This will be the standard method of showing fits to autocorrelation surfaces throughout this article. As described above, we expect in the absence of flow that $\tau_F \rightarrow \infty$, which corresponds to $v_F \rightarrow 0$. A fit to Eq. 21 gives $\tau_D = 0.77 \pm 0.02$ ms and a flow speed $v_F = 0.0 \pm 1.3$ μm/s, which indicates the absence of flow. The fitted value for the flow angle is $110 \pm 690°$. In other words, no flow direction is discernible from the data as expected for random diffusion. The correlation function is independent of phase angle ϕ,

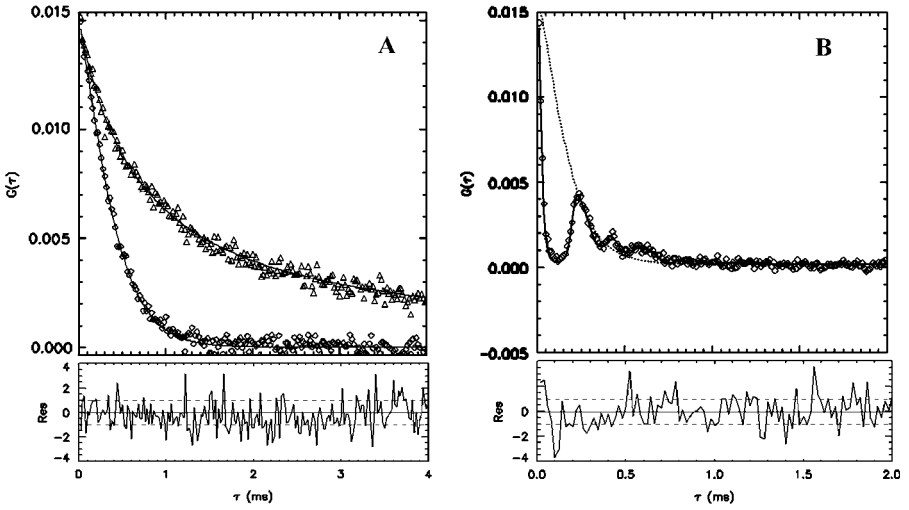

FIGURE 6 FCS and SFCS flow measurement of an Alexa488 water/glycerol solution. (*A*) The FCS correlation function (△) was measured in the absence of flow. Fitting of the data determined a diffusion time of $\tau_D = 0.72 \pm 0.02$ ms. The diamonds represent the FCS correlation function measured in the presence of flow. The fit determined a flow time of $\tau_F = 0.64 \pm 0.01$ ms. The residuals of the fit to the data in the presence of flow are shown below and give a reduced χ^2 of 1.6. (*B*) SFCS correlation function (◇) of the flowing sample was fit to theory. The fit returns a flow time of $\tau_F = 0.61 \pm 0.01$ ms (reduced $\chi^2 = 1.6$). The residuals to the fit are graphed below. The dotted line shows the fit to the corresponding FCS correlation function as reference. The SFCS correlation function exceeds the regular FCS function at later times as predicted by theory.

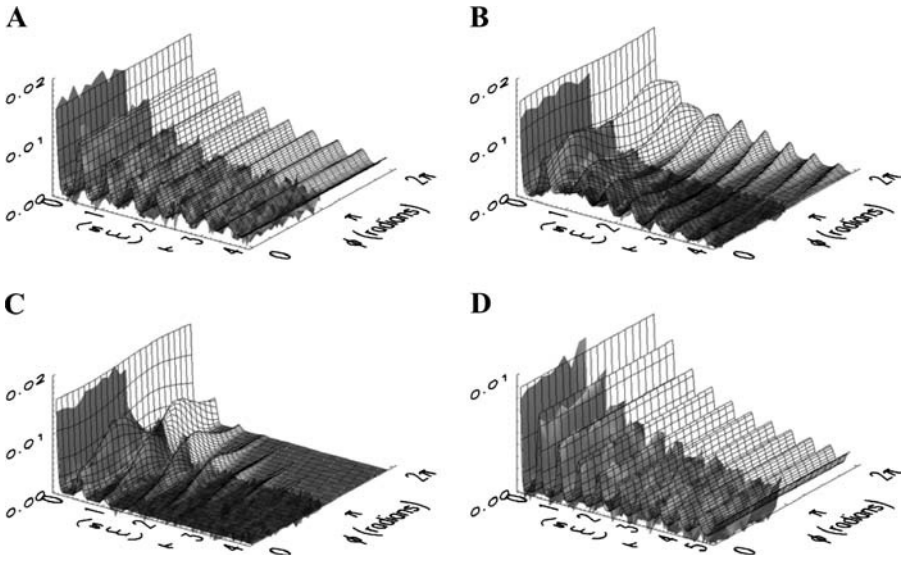

FIGURE 7 PSFCS correlation functions. The experimental correlation functions are only shown for phase angles from 0 to π. The mesh represents the fit of the experimental data to theory. (*A*) PSFCS correlation function of diffusing Alexa488. The fit of the experimental data to theory determines a diffusion time of $\tau_D = 0.77 \pm 0.02$ ms. The amplitude of the correlation function is independent of phase as expected for diffusion. (*B*) PSFCS correlation function of Alexa488 flowing inside a capillary. The fit determines a flow angle of $\theta_F = 175.3 \pm 0.6°$ with a reduced χ^2 of 1.6. (*B*) PSFCS correlation function of Alexa488 with reversed flow direction. Fitting results in a flow angle of $\theta_F = -5.50 \pm 0.52°$. (*D*) PSFCS correlation function of EGFP in vivo. The correlation function is fit by a diffusion-only model with $\tau_D = 0.75 \pm 0.02$ ms.

because diffusion of the dye is isotropic. A fit of the experimental correlation function to Eq. 22, which models the case of pure diffusion, leads to the same correlation surface as shown in Fig. 7 *A*, and results in a diffusion time of $\tau_D = 0.77 \pm 0.02$ ms and a reduced χ^2 of 1.4.

Next we use PSFCS to determine the direction of flow as well as its velocity by analyzing data taken with flow present. The capillary is positioned so that forward flow through it corresponds to an angle of $\sim\pi$. Fig. 7 *B* shows the experimentally determined correlation function and the best fit to Eq. 21. The experimental data clearly show the fastest decay for a phase of $\sim\pi$, which agrees with the experimentally chosen direction. The fit determined a flow time of $\tau_F = 0.97 \pm 0.01$ ms, which corresponds to a flow velocity of 0.359 ± 0.031 mm/s, and a direction of $175.3 \pm 0.6°$. For an independent determination of the flow speed the duration of the experiment was timed and the volume of fluid passing through the capillary measured. These numbers were used to estimate the flow velocity at a distance of 20 μm from the capillary wall, which corresponds to *z*-position of the experiment, assuming a parabolic profile of the flow velocity within the capillary. We estimated a flow velocity of ~0.32 mm/s, which agrees well with the fitted value.

Now we reversed the direction of flow without touching the capillary and increased the flow speed to an estimated value of ~0.62 mm/s. Fig. 7 *C* shows the experimentally determined correlation function and the fit. The data show the fastest decay for a phase of ~0, which agrees with reversing the flow direction. Overall, the correlation decays faster than the function presented in Fig. 7 *B*, indicating the larger flow speed. Fitting reveals a flow speed of 0.569 ± 0.050 mm/s and a direction of $\theta_F = -5.50 \pm 0.52°$. The flow speed agrees within 1.2σ with the independently estimated flow velocity of 0.62 mm/s. In addition, the fitted phase angles differ by 180.8°, which is in excellent agreement with reversing the direction of flow.

PSFCS in vivo

To demonstrate the feasibility of performing position-sensitive SFCS inside of cells, we measured EGFP in the nucleus of COS-1 cells using a scan radius of 0.4 μm and a frequency of 2 kHz. The experimental correlation function is shown in Fig. 7 *D* together with a fit to Eq. 21. We fit the data to determine a scaled radius of 1.14 ± 0.01 and a diffusion time of 0.75 ± 0.02 ms. The flow velocity from the fit is 1.8 ± 1.4 μm/s, and a flow direction of $\theta_F = -31 \pm 43°$ with a reduced χ^2 of 1.6. Because we know the scan radius from calibration, we used the fitted value for the scaled radius to calculate the beam waist $w_0 = r_s/\rho$. Using this beam waist to calculate the diffusion coefficient from the fitted diffusion time, we obtain $D \sim 20$ $\mu m^2/s$. This value is in good agreement with measurements for nuclear EGFP in HeLa cells quoted in the literature (14). The magnitude and the errors for the flow parameters, τ_F and θ_F, indicate that the data are independent of flow. Fitting of the data to a model without flow (Eq. 22) describes the data within experimental accuracy, yielding the same scaled radius and diffusion time quoted above for the model that includes flow and a reduced χ^2 of 1.6. The correlation function shown in Fig. 7 *D* is independent of phase angle as expected for diffusion.

Immobilization

We now apply SFCS and PSFCS to immobilized particles. A fluorescent sphere is immobilized on a coverslip and measured using a scan radius of 0.4 μm at 2 kHz, which corresponds to a scaled radius of 1.3. Fig. 8 *A* shows the SFCS correlation function (*diamonds*) and its fit to Eq. 26 (*solid line*). The fit determined a distance of 0.35 ± 0.01 μm from the center of the scan for the immobilized particle. We also calculated the PSFCS autocorrelation function of the same data according to Eq. 18 (see Fig. 8 *B*). As is the case for the

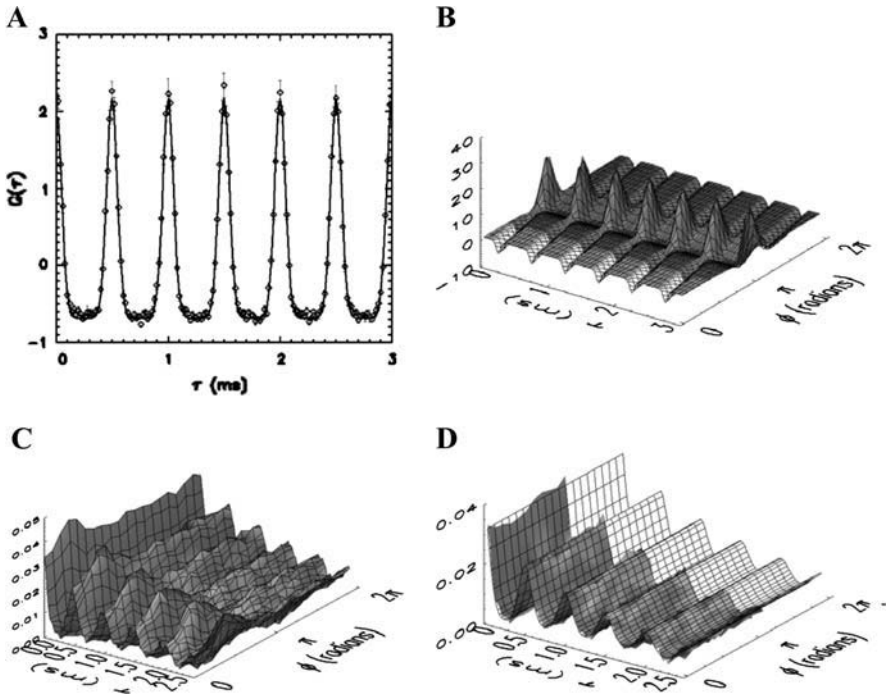

FIGURE 8 Correlation functions of an immobilized fluorescent sphere. (*A*) The SFCS correlation function (◇) is fit to Eq. 26. The fit with a reduced χ^2 of 1.4 is shown as solid line and determines the radial position of the particle as $r_p = 0.35 \pm 0.01$ μm from the center of the scan. (*B*) The PSFCS correlation function of the same experiment is shown. Fitting of the data determines both the radial and angular position of the particle; $r_p = 0.34 \pm 0.01$ μm and $\theta_F = 173.1 \pm 0.1°$ ($\chi^2 = 1.4$). (*C*) PSFCS correlation function of the immobilized sphere in the presence of a diffusing dye solution. The periodic peaks characterize the presence of the immobile particle, whereas the decaying, wavelike structure is indicative of the diffusing dye solution. (*D*) Phase-normalized PSFCS correlation function of the same data as shown in panel C. The periodic peaks of the immobile particle are absent. Fitting of the correlation function to a diffusion-only model yields a reduced χ^2 of 1.3 with a diffusion time of $\tau_D = 0.89 \pm 0.01$ ms.

SFCS correlation function, periodic peaks are visible. Their maximal amplitude is found for a phase of approximately π, which characterizes the angular position of the particle. Fitting to Eq. 25 yields $\theta = 173.7 \pm 0.1°$ and $r_p = 0.34 \pm 0.01$ μm. The radial distance of the particle determined by SFCS and PSFCS agrees within 1σ.

Next, we measure a mixture where an immobilized and a diffusing species are present. In this case the choice of normalization for the position-sensitive SFCS is very important and has a dramatic effect on the autocorrelation function. A sample containing immobilized spheres and a solution of diffusing dye was scanned. Position-sensitive correlation functions were determined using both standard and angle-dependent normalization as defined in Eqs. 18 and 19. Fig. 8 *C* shows the autocorrelation function for standard normalization of the mixture, and Fig. 8 *D* presents the correlation function using angle-dependent normalization. The correlation function in Fig. 8 *C* exhibits peaks at a phase of $\sim\pi/2$, which are due to an immobilized particle. In addition, the function shows a periodic wave-like structure, which is due to the diffusing particles. The periodic peaks are absent for the phase-normalized correlation function in Fig. 8 *D*. We are left with a phase-independent correlation function indicative of diffusion. Immobilized particles result in a vanishing phase-normalized correlation function. In other words, phase-sensitive normalization allows us to focus on dynamic processes and eliminate static or immobilized sources of fluorescence. The correlation function of the mixture is, according to Eq. 28, given by,

$$\tilde{G}_{\text{mixture},\phi}(\phi,\tau) = \frac{\langle F_{\text{diff}}\rangle^2}{\langle F_{\text{tot}}\rangle_\phi \langle F_{\text{tot}}\rangle_{\phi+\omega\tau}} \tilde{G}_{\text{diff},\phi}(\phi,\tau), \qquad (29)$$

where $\langle F_{\text{diff}}\rangle$ is the average fluorescence intensity and $\tilde{G}_{\text{diff},\phi}(\phi,\tau)$ is the correlation function of the diffusing species. Because the fluorescence intensities $\langle F_{\text{diff}}\rangle$ and $\langle F_{\text{tot}}\rangle$ are similar, we approximate Eq. 29 by setting the fractional intensity prefactor to one and fit the correlation function of the mixture to $\tilde{G}_{\text{diff},\phi}(\phi,\tau)$ as defined by Eq. 21. We obtain a reduced χ^2 of 1.3 and a diffusion time of $\tau_D = 0.89 \pm 0.01$ ms, which agrees with the result from regular FCS measurement taken as a control on the same sample.

DISCUSSION

We introduced PSFCS to fully harness the spatial information contained in SFCS measurements. We presented the theory of PSFCS and discussed three specific systems: diffusion, diffusion in the presence of uniform flow, and immobilization. The technique applied to a diffusing dye solution verified the isotropic nature of the system. PSFCS was used to measure the direction and speed of a dye solution flowing through a capillary. We determined the flow direction to within a degree, which highlights the directional sensitivity of the PSFCS technique.

We introduced two different position-sensitive correlation functions, which use different averages of the fluorescence. The standard position-sensitive correlation function $G_\phi(\phi,\tau)$ utilizes the time-averaged fluorescence intensity $\langle F\rangle$, whereas the phase-normalized position-sensitive correlation function $\tilde{G}_\phi(\phi,\tau)$ uses the average fluorescence $\langle F\rangle_\phi$ at the phase angle ϕ. Both definitions of the correlation function are identical if the average fluorescence is independent of the phase, $\langle F\rangle_\phi = \langle F\rangle$, as is the case for diffusion and flow.

However, a stationary particle introduces an angle-dependent fluorescence signal. As we discussed earlier the phase-normalized correlation function of an immobilized particle vanishes, whereas the standard position-sensitive correlation function shows characteristic peaks that we used to determine the position of an immobilized sphere. This different behavior of the two correlation functions is also important when analyzing PSFCS data, where both diffusing and immobilized particles are present. The standard PSFCS correlation function contains correlations from both the diffusing and stationary particles. The phase-normalized PSFCS correlation function, on the other hand, removes all correlations from stationary sources. It is important to note, however, that the influence of the stationary sources is not completely eliminated by using the phase-dependent PSFCS function. The amplitude of the correlation function is still modulated by the phase-dependent fractional intensity prefactor (see Eq. 29). It is possible to incorporate the prefactor into the fitting algorithm, although we have not demonstrated this here. Instead, we set the prefactor to 1, because the variation of the fluorescence intensity as a function of phase was on the order of 10%. This approximation resulted in a good fit of the data with a reduced χ^2 close to 1.

PSFCS correlation functions are converted to SFCS correlation functions by averaging over all phase angles. The SFCS correlation function for diffusion has been previously described for a circular scan path (4). We successfully used their theory to determine the diffusion time of a diffusing dye by fitting the entire SFCS correlation curve. Previously, only the envelope of the SFCS correlation function was fit, which is described by FCS theory. Fitting of the envelope does not use the full information of the SFCS correlation function and is not appropriate for a flowing sample. For this case the SFCS correlation function is not enveloped by the FCS correlation function (Fig. 1 *B*) and therefore one must fit the entire SFCS correlation function. We extended SFCS theory by developing expressions for flow and immobilized particles. We applied this theory to determine the flow velocity of a sample and the radial distance of an immobilized particle by fitting SFCS data.

SFCS is attractive because it can reduce the effect photobleaching has on the autocorrelation function. In FCS measurements, photobleaching causes an apparent decrease in the diffusion time because once bleached, a molecule stops fluorescing while it is still within the observation volume. Because the probability of photodamage increases with exposure time, scanning the beam causes a reduction in the amount of photobleaching at any one particular volume. Therefore, bleaching will affect a fewer number of fluorophores in any given volume resulting in a more accurate measurement of the residence time. We conducted a power study using EGFP in aqueous solution to compare the effect of photobleaching on FCS and SFCS. At higher power, photobleaching is quite easily seen. The FCS curve does not envelope the SFCS curve as expected for pure diffusion (see Fig. 5). We found that the diffusion time determined from FCS was ~25% smaller at the higher power. Using SFCS the effect was reduced to ~5%, which was within the experimental uncertainty of the measurement at lower power. A previous study of photobleaching, conducted on dyes, showed that adding antioxidants such as ascorbic acid can be used to reduce photodamage (15). However, in many cases, altering samples in this manner is not an option as it may modify the behavior of the system under study. For in vivo measurements the addition of antioxidants is not a feasible solution. SFCS reduces the effect of photodamage without altering the sample, which is an inherent advantage of SFCS over the FCS technique.

PSFCS requires synchronization between scanning and data acquisition so that the position of the excitation beam is known at all times. Regular SFCS experiments, on the other hand, do not require synchronization, because correlations are calculated independent from beam position. The response of the galvanometer scanner is frequency dependent and requires calibration measurements to determine the absolute position of the beam at the sample with respect to the driving signal. We determined the scan radius and the absolute phase angle with respect to a chosen laboratory frame using a position sensitive device mounted on the microscope. A detailed description of the calibration of the scanner with the PSD has been presented elsewhere (16). The scanner calibration and the measured beam waist allowed us to determine the scaled scan radius ρ, which we used for fitting data. We alternatively measured a sample with a diffusion time known from an independent FCS experiment and used its value to determine the scan radius by fitting the SFCS correlation function. Both methods yielded the same scan radius within experimental error.

When conducting our experiments we chose parameters that would best mimic conditions encountered in the cell. The Alexa488 dye was slowed in the glycerol solution to obtain diffusion times $\tau_D \sim 0.5$ ms. This is comparable to the diffusion time found for cellular proteins, an example of which is the EGFP data presented above. The mechanical limitations of the scanner place limitations on the minimum diffusion coefficient measurable. Our galvo-scanner is limited to scan periods of ~0.3 ms, which suggests a lower limit on the diffusion time of 0.1 ms. This corresponds to an upper limit on the diffusion coefficient of ~120 $\mu m^2/s$, and is sufficient for cellular studies. Measurements of dyes in solution ($D \sim 300\ \mu m^2/s$) present the fastest diffusion time one would practically encounter. A resonant scanner with a frequency of ~8 kHz would be adequate for such studies.

FCS and related techniques have been used to characterize flow in the past. Shortly after FCS was introduced, it was applied to systems in which flow or sample translation occurred (11). More recently, FCS has found applications for measuring flow in capillary electrophoresis experiments and in microfluidic structures (17–21). Because FCS is not sensitive to the flow direction, variations of the technique

have been introduced to sense direction. For example, by putting a slit in the excitation beam path the *x-y* symmetry of the observation volume is broken, making the decay rate of the autocorrelation function sensitive to the angle at which the slit is positioned with respect to the excitation beam. (22). However, the method requires multiple measurements taken at different slit angles to determine the flow direction. A spatial cross-correlation technique sensitive to flow direction has also been introduced (23–25). In this method two stationary volumes are excited and the cross-correlation function between them is computed. This technique is sensitive to the flow component along the direction of the two excitation volumes. PSFCS has the advantage that it determines the absolute direction of flow within the plane defined by the scan path. We demonstrated an angular resolution of $\sim 1°$ with PSFCS. Note that all techniques discussed are essentially insensitive to flow along the axial direction.

PSFCS has been developed to use the spatial and temporal information embedded in scanning FCS experiments. The technique most similar to PSFCS was developed by Koppel and co-workers in which a single line was repeatedly scanned to create images as a function of both space and time (7). Correlations were calculated simultaneously in space and time. However, the technique probes along a single direction making it insensitive to flow perpendicular to the scan axis. The method is also relatively slow, because the repositioning of the beam for each line scan is time consuming. Another technique that is able to incorporate spatial and temporal correlations is image correlation spectroscopy (26,27). The technique has been mainly used to calculate correlations in space only, although the averaged temporal autocorrelation function of images has been obtained as well (28). Recently, a combination of spatial and temporal image correlation spectroscopy has been used to study the dynamics and clustering of membrane adhesion proteins involved in cell migration (29). The limited time resolution of the technique makes it best suited for systems with slow dynamics. Another study employed SFCS to study protein-membrane interactions with giant unilamellar vesicles (6). However, spatial and temporal correlations were not calculated simultaneously. Separate temporal correlations were calculated for each point along a circular scan circumference traversing the vesicle membrane. These correlations were then fit to the standard FCS theory for stationary volumes.

FCS cannot detect immobilized particles. Their fluorescence adds to the background without introducing fluctuations. This reduces the measured fluctuation amplitude for a diffusing sample in the presence of immobilized particles and leads to a bias in the calculation of the concentration. PSFCS is useful, because it detects immobilized particles and in principle allows the simultaneous characterization of the mobile and immobile fraction of a sample. This is particularly useful for cellular applications, where binding to large structures leads to an effective immobilization on the timescale of the experiment. So far immobilization has not been considered when applying FCS in cells. We will explore in the future the potential of PSFCS to characterize proteins in living cells. For the moment we restrict ourselves to a PSFCS measurement of EGFP in cells to demonstrate the feasibility of intracellular applications.

CONCLUSION

We introduced PSFCS and calculated correlations in both space and time. We demonstrated that PSFCS determines the direction of flow and the position of a stationary particle. We also established the feasibility of applying the technique to intracellular studies by measuring EGFP in COS cells. In addition, we presented an example of applying PSFCS to a more complicated system that contains a mixture of mobile and immobile particles. Within the cellular environment, it is not unreasonable to expect the presence of such immobilized particles within the timeframe of single measurement (~ 1 min). PSFCS has the potential to aid in characterizing mobile and immobile proteins in cells.

This work was supported by grants from the National Institutes of Health (GM64589) and the National Science Foundation (PHY-0346782). Y.C. acknowledges support from a postdoctoral fellowship from the National Institutes of Health (GM020853).

REFERENCES

1. Elson, E. L., and D. Madge. 1974. Fluorescence correlation spectroscopy. I. Conceptual basis and theory. *Biopolymers.* 12:1–27.
2. Weissman, M., H. Schindler, and G. Feher. 1976. Determination of molecular weights by fluctuation spectroscopy: application to DNA. *Proc. Natl. Acad. Sci. USA.* 73:2776–2780.
3. Petersen, N. O., D. C. Johnson, and M. J. Schlesinger. 1986. Scanning fluorescence correlation spectroscopy. II. Application to virus glycoprotein aggregation. *Biophys. J.* 49:817–820.
4. Berland, K. M., P. T. So, Y. Chen, W. W. Mantulin, and E. Gratton. 1996. Scanning two-photon fluctuation correlation spectroscopy: particle counting measurements for detection of molecular aggregation. *Biophys. J.* 71:410–420.
5. Petersen, N. O. 1986. Scanning fluorescence correlation spectroscopy. I. Theory and simulation of aggregation measurements. *Biophys. J.* 49:809–815.
6. Ruan, Q., M. A. Cheng, M. Levi, E. Gratton, and W. W. Mantulin. 2004. Spatial-temporal studies of membrane dynamics: scanning fluorescence correlation spectroscopy (SFCS). *Biophys. J.* 87:1260–1267.
7. Koppel, D. E., F. Morgan, A. E. Cowan, and J. H. Carson. 1994. Scanning concentration correlation spectroscopy using the confocal laser microscope. *Biophys. J.* 66:502–507.
8. Meyer, T., and H. Schindler. 1988. Particle counting by fluorescence correlation spectroscopy. Simultaneous measurement of aggregation and diffusion of molecules in solutions and in membranes. *Biophys. J.* 54:983–993.
9. Berland, K. M., P. T. So, and E. Gratton. 1995. Two-photon fluorescence correlation spectroscopy: method and application to the intracellular environment. *Biophys. J.* 68:694–701.
10. Thompson, N. L. 1991. Fluorescence correlation spectroscopy. *In* Topics in Fluorescence Spectroscopy. J. R. Lakowicz, editor. Plenum. New York, NY. 337–378.

11. Magde, D., W. W. Webb, and E. L. Elson. 1978. Fluorescence correlation spectroscopy. III. Uniform translational and laminar flow. *Biopolymers.* 17:361–376.

12. Patterson, G. H., S. M. Knobel, W. D. Sharif, S. R. Kain, and D. W. Piston. 1997. Use of the green fluorescent protein and its mutants in quantitative fluorescence microscopy. *Biophys. J.* 73:2782–2790.

13. Bevington, P. R., and D. K. Robinson. 1992. Data Reduction and Error Analysis for the Physical Sciences. McGraw-Hill, New York, NY.

14. Chen, Y., J. D. Müller, Q. Ruan, and E. Gratton. 2002. Molecular brightness characterization of EGFP in vivo by fluorescence fluctuation spectroscopy. *Biophys. J.* 82:133–144.

15. Dittrich, P. S., and P. Schwille. 2001. Photobleaching and stabilization of fluorophores used for single-molecule analysis with one- and two-photon excitation. *Appl. Phys. B.* 73:829–837.

16. Skinner, J. P., Y. Chen, and J. D. Muller. 2005. Position-sensitive scanning fluorescence correlation spectroscopy. *Proc SPIE.* 5700:118–127.

17. Kunst, B. H., A. Schots, and A. J. Visser. 2002. Detection of flowing fluorescent particles in a microcapillary using fluorescence correlation spectroscopy. *Anal. Chem.* 74:5350–5357.

18. Dittrich, P. S., and P. Schwille. 2003. An integrated microfluidic system for reaction, high-sensitivity detection, and sorting of fluorescent cells and particles. *Anal. Chem.* 75:5767–5774.

19. Gosch, M., H. Blom, J. Holm, T. Heino, and R. Rigler. 2000. Hydrodynamic flow profiling in microchannel structures by single molecule fluorescence correlation spectroscopy. *Anal. Chem.* 72:3260–3265.

20. Van Orden, A., and R. A. Keller. 1998. Fluorescence correlation spectroscopy for rapid multicomponent analysis in a capillary electrophoresis system. *Anal. Chem.* 70:4463–4471.

21. Foquet, M., J. Korlach, W. Zipfel, W. W. Webb, and H. G. Craighead. 2002. DNA fragment sizing by single molecule detection in submicrometer-sized closed fluidic channels. *Anal. Chem.* 74:1415–1422.

22. Lenne, P.-F., D. Colombo, H. Giovannini, and H. Rigneault. 2002. Flow profiles and directionality in microcapillaries measured by fluorescence correlation spectroscopy. *Single Mol.* 4:194–200.

23. LeCaptain, D. J., and A. Van Orden. 2002. Two-beam fluorescence cross-correlation spectroscopy in an electrophoretic mobility shift assay. *Anal. Chem.* 74:1171–1176.

24. Fogarty, K., and A. Van Orden. 2003. Two-beam fluorescence cross-correlation spectroscopy for simultaneous analysis of positive and negative ions in continuous-flow capillary electrophoresis. *Anal. Chem.* 75:6634–6641.

25. Dittrich, P. S., and P. Schwille. 2002. Spatial two-photon fluorescence cross-correlation spectroscopy for controlling molecular transport in microfluidic structures. *Anal. Chem.* 74:4472–4479.

26. Petersen, N. O., P. L. Hoddelius, P. W. Wiseman, O. Seger, and K. E. Magnusson. 1993. Quantitation of membrane receptor distributions by image correlation spectroscopy: concept and application. *Biophys. J.* 65:1135–1146.

27. Wiseman, P. W., and N. O. Petersen. 1999. Image correlation spectroscopy. II. Optimization for ultrasensitive detection of preexisting platelet-derived growth factor-beta receptor oligomers on intact cells. *Biophys. J.* 76:963–977.

28. Wiseman, P. W., J. A. Squier, M. H. Ellisman, and K. R. Wilson. 2000. Two-photon image correlation spectroscopy and image cross-correlation spectroscopy. *J. Microsc.* 200:14–25.

29. Wiseman, P. W., C. M. Brown, D. J. Webb, B. Hebert, N. L. Johnson, J. A. Squier, M. H. Ellisman, and A. F. Horwitz. 2004. Spatial mapping of integrin interactions and dynamics during cell migration by image correlation microscopy. *J. Cell Sci.* 117:5521–5534.